PNAS

Supporting Information for

High-Entropy Engineering with Regulated Defect Structure and Electron Interaction Tuning Active Sites for Trifunctional Electrocatalysis

Xiaoxiao Zou[a], Jiyang Xie[a], Zhiyuan Mei[a], Qi Jing[a], Xuelin Sheng[a], Conghui Zhang[a], Yongxin Yang[a], Mengjiao Sun[a], Futong Ren[a], Lilian Wang[a], Tianwei He[a,*], Youchao Kong[b,*], Hong Guo[a,c,*]

[a] School of Materials and Energy, International Joint Research Center for Advanced Energy Materials of Yunnan Province, Yunnan Key Laboratory of Carbon Neutrality and Green Low-carbon Technologies, Yunnan University, No. 2, Green Lake North Road, Kunming 650091, China

[b] Department of Physics and Electronic Engineering, Yancheng Teachers University, Yancheng 224002, China

[c] Southwest United Graduate School, Kunming 650091, China

*To whom correspondence may be addressed.
Email:
guohong@ynu.edu.cn (H. G.); yb87816@um.edu.mo (Y. K.); he.tianwei@ynu.edu.cn (T. H.)

This PDF file includes:

Supporting Methods

1. Chemicals

All chemical reagents were purchased and used as received without any other purification unless otherwise stated. $FeCl_3$, $NiCl_2$, $CoCl_2$, $CuCl_2$, $PtCl_2$(ACS Reagent Grad), potassium hydroxide (KOH, ≥90%), zinc acetate ($Zn(C_2H_3O_2)_2$, ≥99.5%), ethanol (99.8%), hydrochloric acid (HCl, 36%~38%), commercial Pt/C (20 wt%), and RuO_2 (99.95%) were obtained from Shanghai Titan Scientific Co., Ltd. Nafion solution (5 wt%) was bought from Sigma-Aldrich. Multi-walled carbon nanotubes (MWCNT) (product number TNM5) were purchased from Chengdu Organic Chemicals Co., China. High-purity O_2 (≥99.999%), and high-purity N_2 (≥99.999%), were obtained from Kunminutesg PENGYIDA Gas Products Co. Ltd. Deionized water was prepared by a laboratory water purification system in HHitech Master-S30UVF with a resistivity of 18.2 MΩ·cm at 25 °C was used throughout the experiments.

2. Experimental Section

2.1 The material with high metal loading (50%) is prepared according to the above method and named HHEN/CNT.

2.2 Similarly, a material without metal loading is prepared, named CNT.

3. Characterization.

3.1 Sample characterization.

Powder X-ray diffraction (XRD) was carried out by Rigaku SmartLab SE operated at 40 kV and 50 mA equipped with Cu-Kα radiation with λ=1.5406 Å. The morphology and microstructure of the as-synthesized samples were characterized through transmission electron microscopy (TEM; Talos F200X) and aberration-corrected TEM(AC-TEM) images, and energy dispersive spectroscopy (EDS) were taken on Thermofisher spectra 300, and electron energy loss spectroscopy (EELS) using a Gatan 1065. The elements' molar ratios of the samples were identified by inductively coupled plasma mass spectrometry (ICP-MS, Agilent 5110). Raman spectra were obtained by a HORIBA FRANCE SAS LABRAM HR EVO with the 532 nm excitation line of an Ar ion laser. The unpaired electrons in the atoms or molecules of the sample to see whether vacancy phenomena are produced by Electron Paramagnetic Resonance (EPR) (Bruker, EMXnano). The X-ray absorption fine structure (XAFS) spectroscopy was carried out using the RapidXAFS 1M (Anhui Absorption Spectroscopy Analysis Instrument Co., Ltd.) by transmission mode at 20 kV and 40 mA, and the Si (533) spherically bent crystal analyzer with a radius of curvature of 500 mm was used for Co, the Si (771) spherically bent crystal analyzer with a radius of curvature of 500 mm was used for Pt, the Si (553) spherically bent crystal analyzer with a radius of curvature of 500 mm was used for Cu, the Si (531) spherically bent crystal analyzer with a radius of curvature of 500 mm was used for Fe, the Si (551) spherically bent crystal analyzer with a radius of curvature of 500 mm was used for Ni. The raw XAFS data were calibrated and normalized using the software Demeter.

3.2 Electrochemical test.

Before depositing the electrocatalyst, the electrode was carefully washed and polished to remove all debris and dirt. 3 mg of electrocatalyst was dispersed in 1 mL hybrid solvent containing 0.9mL water and ethanol mixed solution (V_{water}: $V_{ethanol}$=1;1) and 0.1 mL 5wt% Nafion. The as-formed ink was ultrasonically dispersed for 1 h in an iced bath. The electrodes were prepared by dropping 20 μL of catalyst ink on the rotation disk electrode (RDE, 5 mm in diameter with an exposed area of 0.196 cm^2) and drying under ambient conditions. Applying a three-electrode mode Ag/AgCl electrode saturated with KCl and carbon rod as a reference and counter electrode, respectively. The potential was calculated concerning the RHE, using the equation (S1):

$$\mathrm{E(RHE)} = \mathrm{E(Ag/AgCl)} + 0.0591 * \mathrm{pH} + 0.197 \quad \text{(S1).}$$

The catalysts were coated onto the rotating disk electrode (RDE) tip serving as the working electrode. the LSV curves were carried at a scan rate of 10 mV s^{-1} and a rotating speed of 1600 rpm. The Tafel slope was obtained by fitting the LSV using Equation (S2):

$$\eta = \mathrm{b}\,(\log \mathrm{j}) + \mathrm{a} \quad \text{(S2).}$$

The overpotential was iR-corrected using Equation (S3):

$$\mathrm{E} = \mathrm{E}\,(\text{applied potential vs. RHE}) - \mathrm{IR} \quad \text{(S3)}$$

where I indicate the current, and R is the ohmic resistance of the electrolyte (≈5 Ω for 1 M KOH, ≈45 Ω for 0.1 M KOH). LSV was performed using a CHI 730e electrochemical workstation and a Pine research instrument. The EIS was measured using an AMETEK PARSTAT3000A-DX electrochemical workstation with a frequency range from 10^5 to 10^{-1} Hz in OCP with 5 mV sinusoidal perturbations. The commercial 20 wt% Pt/C was used as the electrode for ORR and HER. The commercial RuO_2 was used as the electrode for OER. The stability was examined using the chronoamperometry method.

For ORR, the 50-cycle CV scan between 0.2 and 1.0 V vs. RHE at a scan speed of 100 mV s^{-1} was performed to activate the electrocatalyst in an O_2-saturated 0.1 mol KOH solution. The rotating ring-disk electrode (RRDE) measurements were performed at the voltage range from 0.2 to 1.2 V versus RHE in O_2-saturated electrolyte at a rotation speed of 1600 rpm with a scan rate of 10 mV s^{-1}. The electron transfer number (n values) and the HO_2^- formation yields can be calculated from the following equations:

$$n = 4 \times \frac{I_D}{(I_R / N + I_D)} \quad \text{(S4)}$$

$$HO_2^-\% = 200 \times \frac{I_R}{I_D N + I_R} \quad \text{(S5)}$$

where I_D is the disk current, I_R is the ring current, and N is the collection efficiency (0.37).

Before each OER measurement, the 50-cycle CV scan between 0.2 and 0.8 V vs. RHE at a scan speed of 100 mV s^{-1} was performed to activate the electrocatalyst in an O_2-saturated 0.1 mol KOH solution.

The OER Faradaic efficiency (FE) is investigated by the RRDE technique in an N_2-saturated 1M KOH solution at a rotating speed of 1600 rpm. the FE was obtained according to

$$\mathrm{FE} = \mathrm{Iring}/(\mathrm{Ce} \times \mathrm{Idisk}) \quad \text{(S6)}$$

Here, I_{disk} is the given current on the disk electrode. I_{ring} is the collection current on the Pt ring electrode at a constant potential of 0.4 V versus RHE. C_e is the oxygen collection coefficient (~0.37) for this type of electrode configuration.

For HER, the 50-cycle CV scan between 0 and -0.2V vs. RHE at a scan speed of 100 mV s^{-1} was performed to activate the electrocatalyst in an N_2-saturated 1M KOH.

The electrochemical active surface area (ECSA) was determined by comparing the double-layer capacitance (C_{dl}) of the electrocatalysts, where the electrocatalysts with higher C_{dl} exhibit larger ECSA. C_{dl} was measured by cyclic voltammetry (CV) with a scan window between 1.00 and 1.05 V vs. RHE and a series of scan rates of 10, 20, 40, 60, 80, and 100 mV s^{-1}. The linear fitting of the disk current density difference (Δj = (ja – jb)/2) at 1.025 V vs RHE against the scan rates was subsequently performed. C_{dl} was the slope to reveal ECSA.

$$\mathrm{ECSA} = C_{dl}/C_s \quad \text{(S7)}$$

where C_s is the specific capacitance value for a flat standard with 1 cm^2 of real surface area. The general value for C_s is between 20 ~60 μF cm^{-2} Here we use 40 μF cm^{-2} as the average value.

The mass activity (MA) and specific activity (SA) can be calculated from the following equations:

$$\mathrm{MA} = \mathrm{j}/\mathrm{m} \quad \text{(S8)}$$

$$\mathrm{SA} = \mathrm{MA}/\mathrm{ECSA} \quad \text{(S9)}$$

Where m is the loading mass of catalyst per geometrical area of the electrode.

The activity normalized by noble metal mass (MA_{Pt}) using Equation:

$$MA_{Pt} = \mathrm{j}/m_{Pt} \quad \text{(S10)}$$

Where m is the loading mass of Pt for catalyst per geometrical area of the electrode.

An aqueous Zn-air battery was assembled with homemade electrochemical cell frameworks. On the air electrode, the catalyst ink was uniformly coated onto carbon fiber paper at an

effective size of 1.0 × 1.0 cm^2 and then dried at room temperature. The catalyst loading per area was 0.20 $mg \cdot cm^{-2}$ unless otherwise stated. A polished Zn plate was used as the anode with the same effective size. For comparison, the 20%Pt/C and RuO_2-based Zn-air battery (using 20%Pt/C and RuO_2 as ORR and OER electrocatalysts, respectively, and their mass ratio is 1:1) was also assembled and evaluated. The electrolyte was composed of 6 $mol \cdot L^{-1}$ KOH and 0.2 $mol \cdot L^{-1}$ zinc acetate. The battery performance measurements were carried out under a constant current charging-discharging process by a NEWARE Battery Test System (CT-4008-5V50mA-164, Shenzhen, China) at room temperature.

Overall water splitting: A two-electrode system consisted of two carbon cloths loaded with catalysts as both the anode and cathode were conducted to measure water splitting performance. Two carbon cloths dispersed the catalysts ink onto carbon cloth with a loading of 1.0 $mg \cdot cm^{-2}$ and dried to obtain a polarization working curve at a scan rate of 10 mV s^{-1} in 1M KOH electrolyte. For comparison, using 20%Pt/C and RuO_2 as HER and OER electrocatalysts, respectively.

4. Theoretical simulations

Spin-polarized GGA calculations have been performed based on density functional theory (DFT), as implemented in the Vienna ab initio Simulation Package (VASP). [1-2] The Perdew-Burke-Ernzerhof (PBE) function within the generalized gradient approximation was used for the exchange-correlation energy. [3] To avoid the image interaction, the supercells ~12 × 12 × 20 $Å^3$ HEANs slab, Monkhorst-Pack k-point grids of 3 × 3 × 1 respectively, were used during geometry optimization. The cutoff energy for the plan-wave basis was 500 eV. The coverage tolerances for energy and force were set to 10^{-6} eV and 0.02 eV/Å, respectively. Recently developed DFT-D3 method is adopted to include the interaction between the adorsbates and substrates. [4] The model construcution of HEANs was determined by a high-throuput calucation with Python code. The slab for various reactions was cleavged through the miller index of (111), and the bottom two layers were fixed. The implicit solvation model of Mathew et al., named VASPsol was used [5]. For this model we have considered the solvent default parameter. The explicit water model was followed our previous work[6].

4.1 Oxygen Evolution Reaction and Oxygen Reduction Reaction

In case of OER, a complete process involves four concerted proton–electron transfer (CPET) reactions, the reactions in acid condition follow,

R1: $H_2O(l) + * \rightarrow *OH + H^+ + e^-$

R2: $*OH \rightarrow *O + H^+ + e^-$

R3: $*O + H_2O(l) \rightarrow *OOH + H^+ + e^-$

R4: $*OOH \rightarrow * + O_2(g) + H^+ + e^-$

where * represents the reaction site on the surface of catalysts; *OH, *O and *OOH stand for the adsorbed intermediates during the reaction. In respect to ORR, it proceeds in a reversal way to that of OER.

In accordance to the equation $\Delta G = \Delta E + \Delta E_{ZPE} - T\Delta S + \Delta G_U + \Delta G_{pH}$, the free energy difference for elementary steps can be calculated. In this equation, ΔE is the reaction energy defined as the energy difference of reactant and product molecules adsorbed on catalyst surface; $\Delta EZPE$ and ΔS are the changes of zero-point energy and entropy, respectively; $\Delta G_U = -neU$ with U being the applied electrode potential and n the number of electrons transferred; and $\Delta G_{pH} = -k_B T \ln[H^+]$ is the free energy correction of pH.

In this way, thus the free energy barrier for each elementary step can be calculated by

$\Delta G_{R1} = \Delta G_{*OH}$

$\Delta G_{R2} = \Delta G_{*O} - \Delta G_{*OH}$

$\Delta G_{R3} = \Delta G_{*OOH} - \Delta G_{*O}$

$\Delta G_{R4} = 4.92 - \Delta G_{*OOH}$

Here, ΔG_{*OH}, ΔG_{*O} and ΔG_{*OOH} are defined as,

$\Delta G_{*OH} = \Delta G(H_2O + * \rightarrow *OH + H^+ + e^-)$

$\Delta G_{*O} = \Delta G(H_2O + * \rightarrow *O + 2H^+ + 2e^-)$

$\Delta G_{*OOH} = \Delta G(2H_2O + * \rightarrow *OOH + 3H^+ + 3e^-)$

and the overpotential can be obtained through,

$\eta_{OER} = \max(\Delta GR_i), i = 1, 2, 3, 4/e - 1.23$

$\eta_{ORR} = \min(\Delta GR_i), i = 1, 2, 3, 4/e + 1.23$

4.2 Hydrogen Evolution Reaction

In simulation, the overall HER pathway can be described as [7-9],

$$H^+ + e^- \rightarrow \frac{1}{2}H_2, \qquad \Delta G^0 = 0\ eV\ vs.SHE$$

By setting the reference potential to be that of standard hydrogen electrode (SHE), the chemical potential (chemical potential per H) for the initial ($H^+ + e^-$) and final ($1/2 H_2$) states are equal [2]. Hence, the Gibbs free energy of an intermediate adsorbed hydrogen (H*) is an important descriptor for the HER activity of electrocatalyst, and HER performance can be quantified by

the reaction Gibbs free energy of hydrogen adsorption (ΔG_H),

$$\Delta G_H = \Delta E_H + \Delta E_{ZPE} - T\Delta S.$$

where, ΔE_H is the energy difference directly obtained by DFT calculations, which is defined as,

$$\Delta E_H = E[slab + H] - E[slab] - 1/2E[H_2]$$

where $E[\mathrm{slab} + \mathrm{H}]$ and $E[slab]$ represent the total energies of the catalyst adsorbed with and without H atom, respectively. $E[H_2]$ is the energy of H_2. ΔE_{ZPE} - $T\Delta S$ is about 0.24 eV at 298.15K [1], Then, $\Delta G_H = \Delta E_H + 0.24$.

4.3 Surface Pourbaix Diagrams

Surface Pourbaix diagrams reveal the surface states as the function of pH and potential, providing a thermodynamic indication of whether the catalyst will be poisoned. Considering HEANs pristine surface (Slab) with the adsorption site (*) and the pre-adsorbed molecule (O_mH_n*), the adsorption

equation can be written as:

$$Slab - OH* + (2m - n)(e^- + H^+) \rightarrow Slab + mH_2o.$$

where m and n are, respectively, the number of oxygen and hydrogen atoms of the adsorbate. The free energy changes were calculated using:

$$\Delta G = G_{slab} + mG_{H2O} + G_{slab-OH*} - (2m - n)(0.5G_{H2} - U_{SHE} - 0.00591pH)$$

where U_{SHE} is the potential relative to the standard hydrogen electrode (SHE).

Supporting Figures.

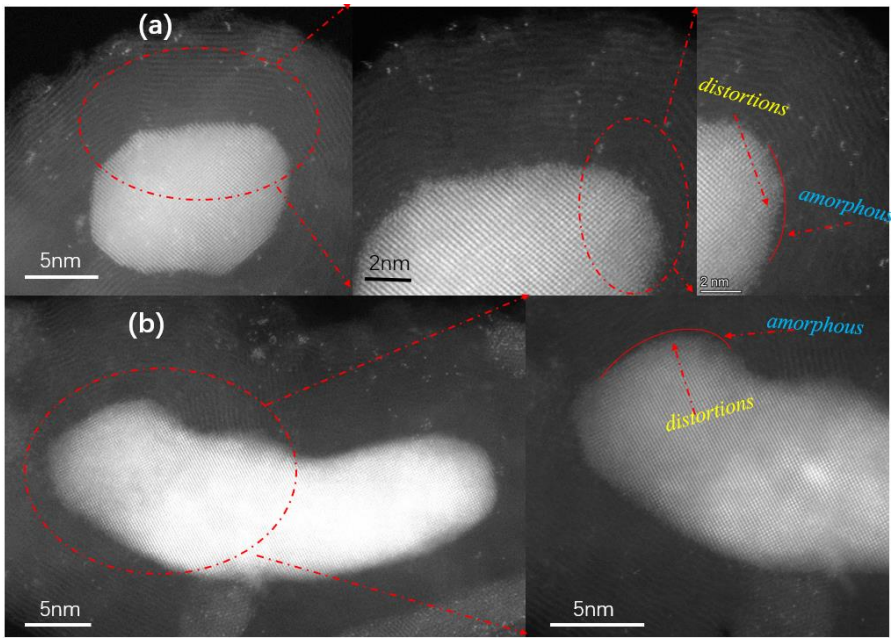

Fig. S1. AC-HAADF-STEM images of metal-C interface interaction for HEAN/CNT.

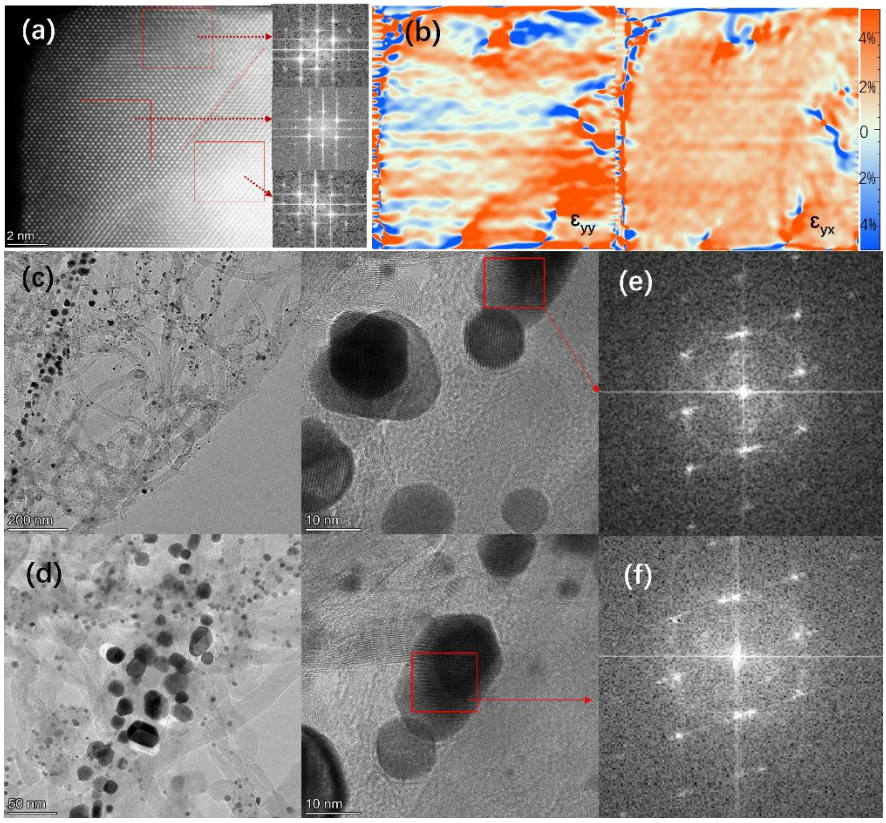

Fig. S2. (a) AC-STEM and the FFT patterns of the relevant parts and (b) GPA images of HEAN/CNT for axial strain (ε_{yy}) and shear strain (ε_{yx}). (c and d) HRTEM images of Pt/CNT, (e and f) the FFT patterns of the relevant parts.

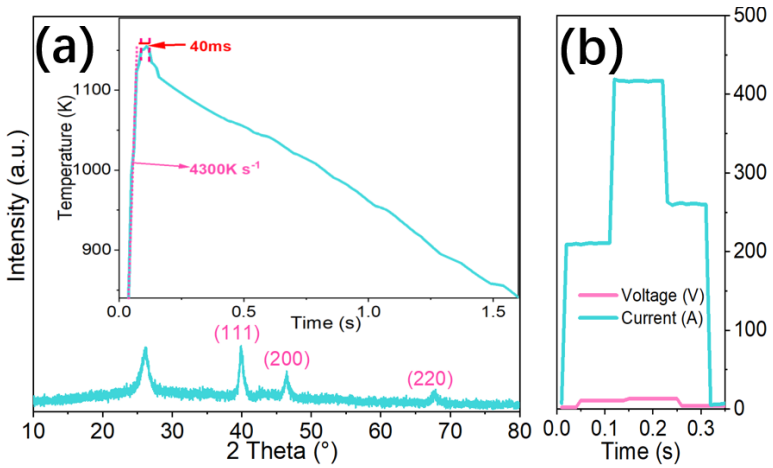

Fig. S3. (a) XRD and the insert picture is preparation temperature (b) the related current and voltage curves of HEAN/CNT.

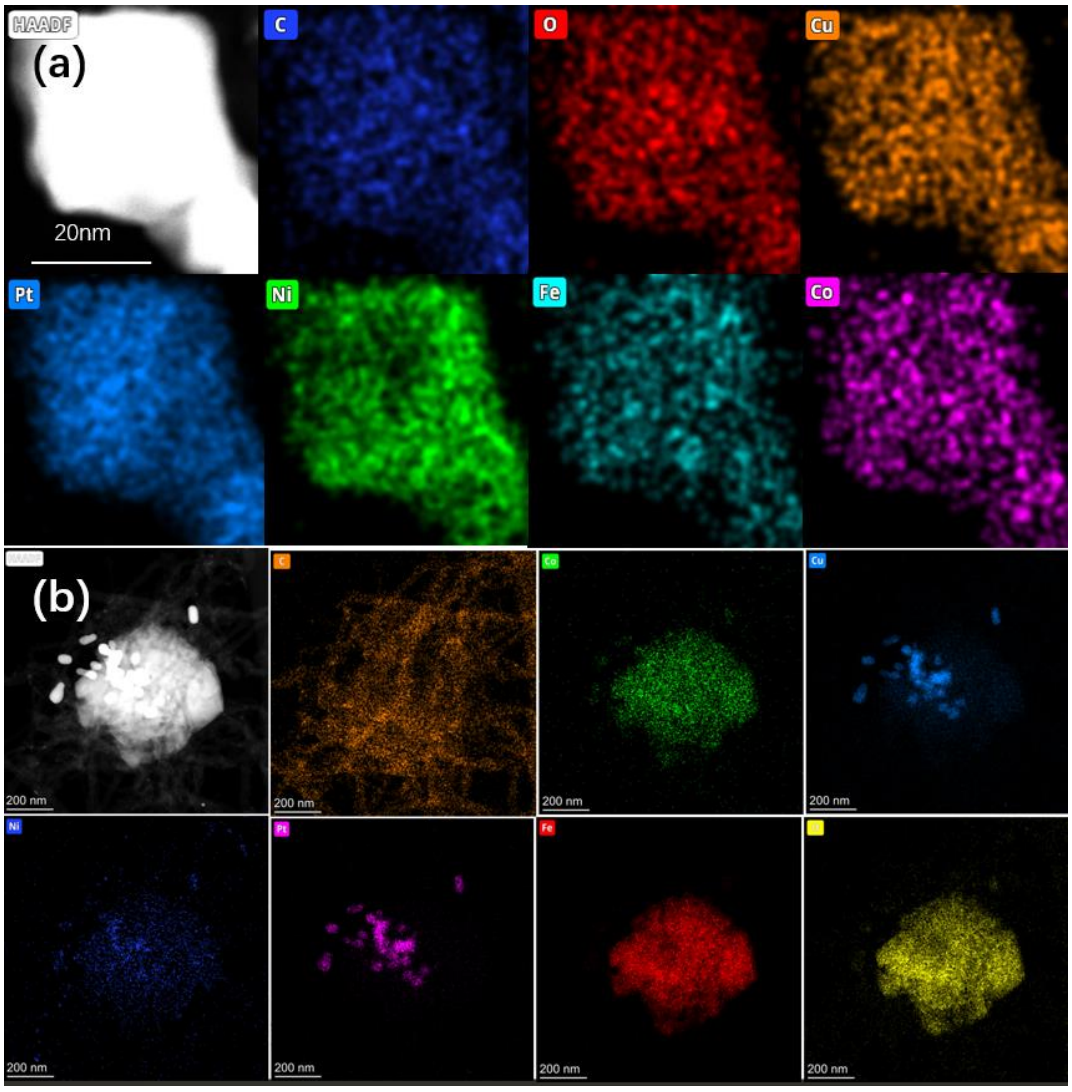

Fig. S4. (a) AC-HAADF and EDS maps for HEAN/CNT, (b) HAADF image and EDS maps of IFHEAN/CNT.

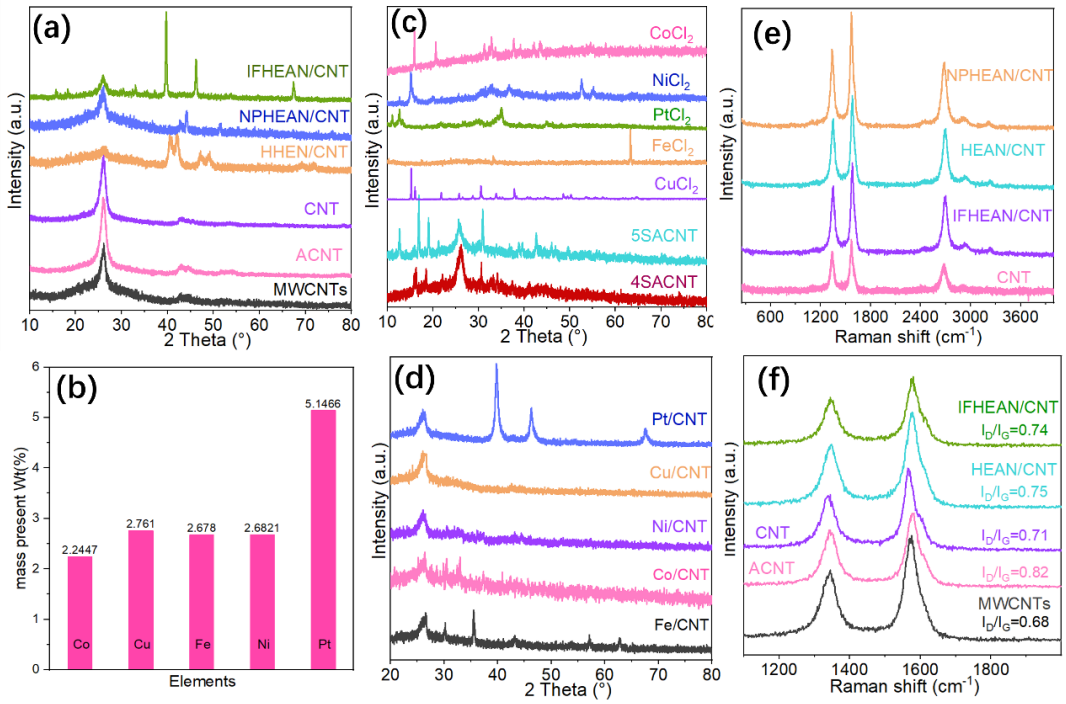

Fig. S5. (a) XRD of different samples, (b)ICP-MS of HEAN/CNT, (c and d) XRD of samples in the preparation process and single metal samples, (e and f) Raman spectra of different samples.

The test results of Raman **(Fig. S5e)** show that no metal oxide peaks were captured, which could also explain the metallic properties of the nanoparticles formed. The carbon structure was analyzed in **Fig. S5f**. Two peaks located at 1340 cm^{-1} and 1580 cm^{-1} are assigned to typical D and G bands of carbon, which correspond to the defects and graphitization degree of carbon materials, respectively. The high intensity of the G band represents a high graphitization degree, which is favorable to the electronic conductivity. The high I_D/I_G value indicates more defect numbers in the carbon frameworks offering more catalytic reaction active sites.

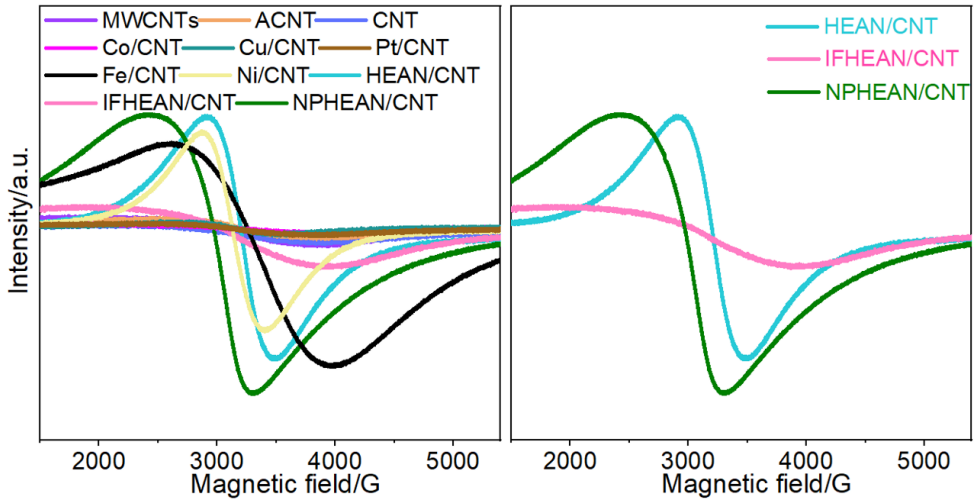

Fig. S6. EPR signals of different samples.

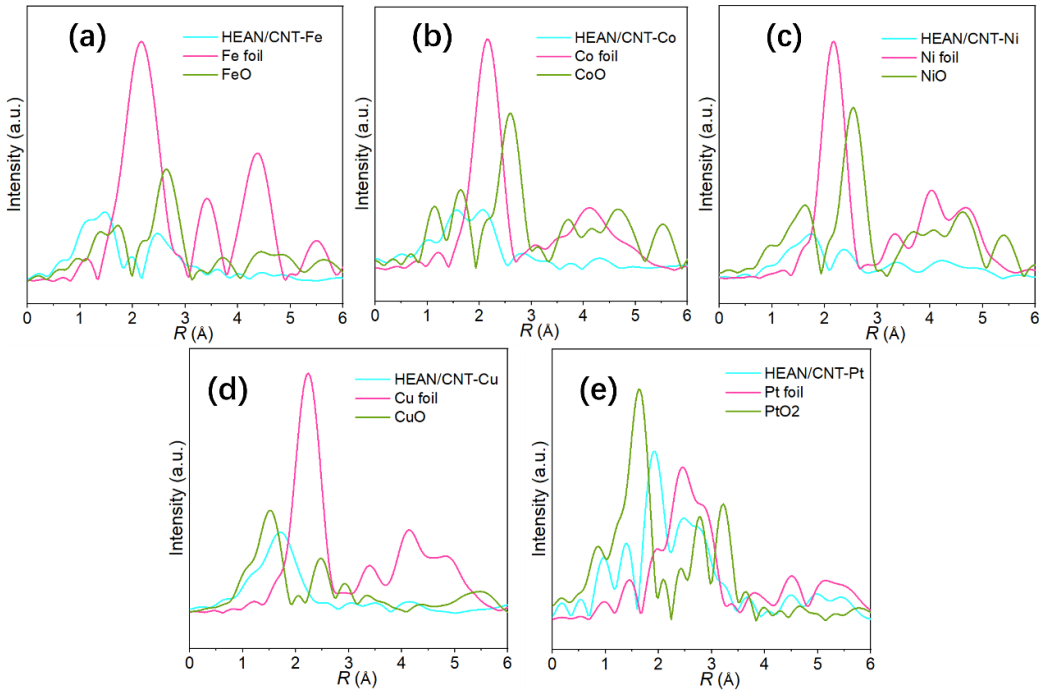

Fig. S7. (a-e) the k3-weighted Fourier transform spectra from EXAFS.

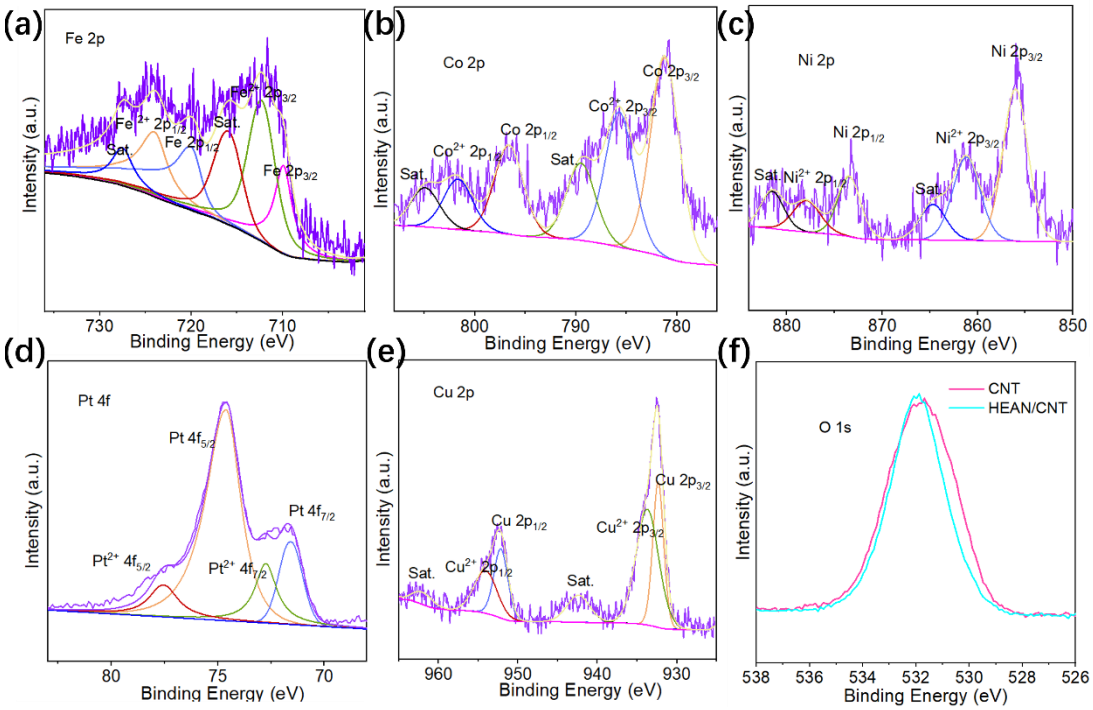

Fig. S8. XPS analysis of HEAN/CNT for (a) Fe 2p spectrum. (b) Co 2p spectrum. (c) Ni 2p spectrum. (d) Pt 4f spectrum. (e) Cu 2p spectrum. (f) O1s spectrum of HEAN/CNT and CNT.

Due to the inevitable exposure to air during the preparation process before XPS measurements results in the oxidation of the catalyst surface. Since XPS only detects the surface composition of the catalyst, metal oxides are observed in the XPS spectra.

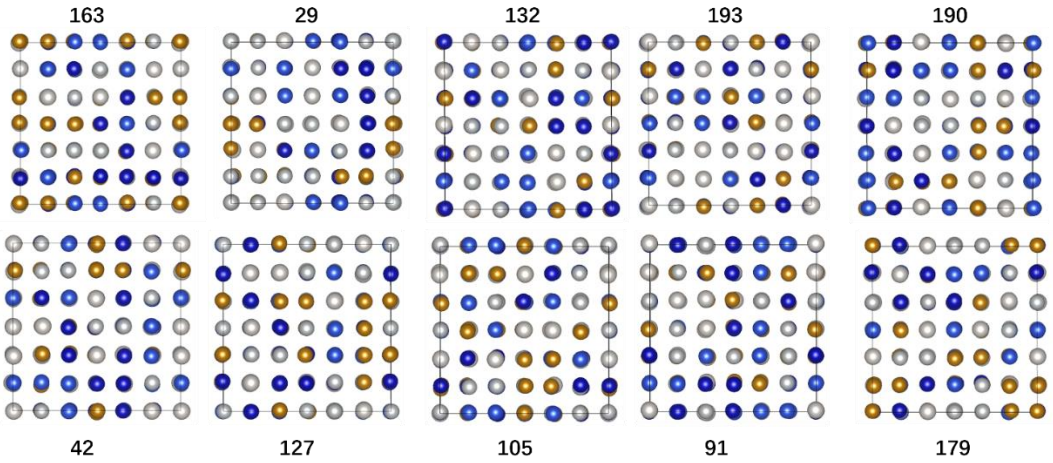

Fig. S9. Top views of ten optimized structures with low energy.

So far, the model construction of high-entropy materials is still a difficult task. Therefore, to be fully considered, we use high-throughput calculations to find the ground states. In our work, for the model construction and selection of HEANs, we employed Python code embedded in the Atomic Simulation Environment (ASE), which is an ASE written in the Python programming language with the aim of setting up, steering, and analyzing atomistic simulations, to construct the HEANs models. Firstly, we randomly replaced platinum with Fe, Co, Ni, and Cu to form 250 HEANs stochastic structures for first-step optimization calculations. The energies of the 250 HEANs are listed in **Table S2**. We then selected the 10 structures with the lowest energies among the 250 structures for the next step high-precision optimization (**Fig. S9**). Finally, after high precision optimization, the No.179 with the lowest energy was selected as a candidate for the following calculations (**Fig. 3g**).

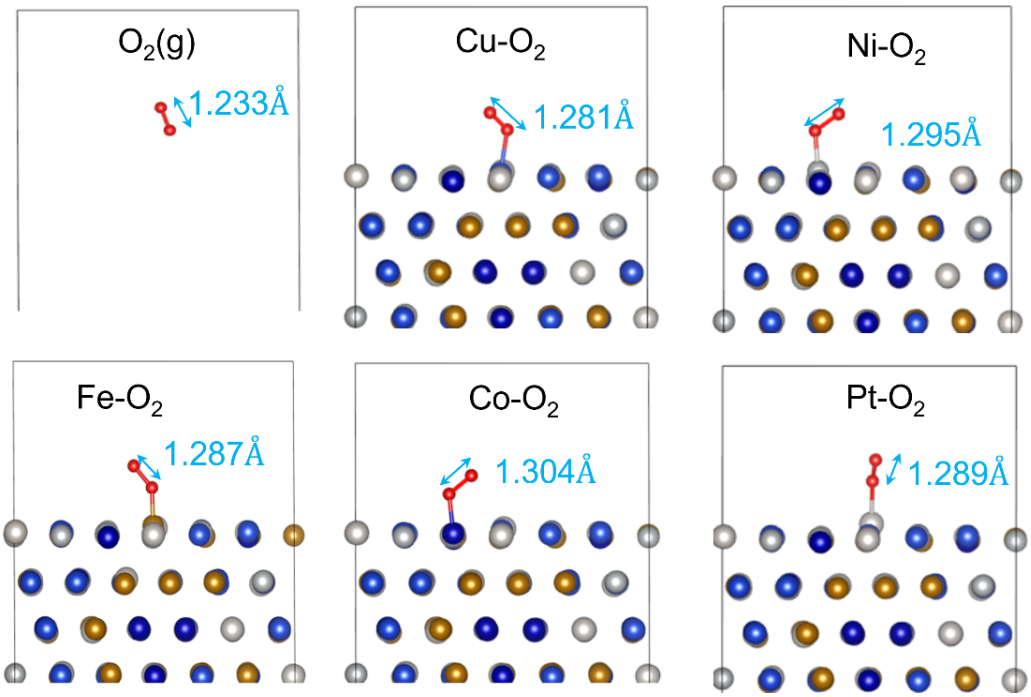

Fig. S10. Optimized structure of O_2 adsorbed on active sites of HEANs.

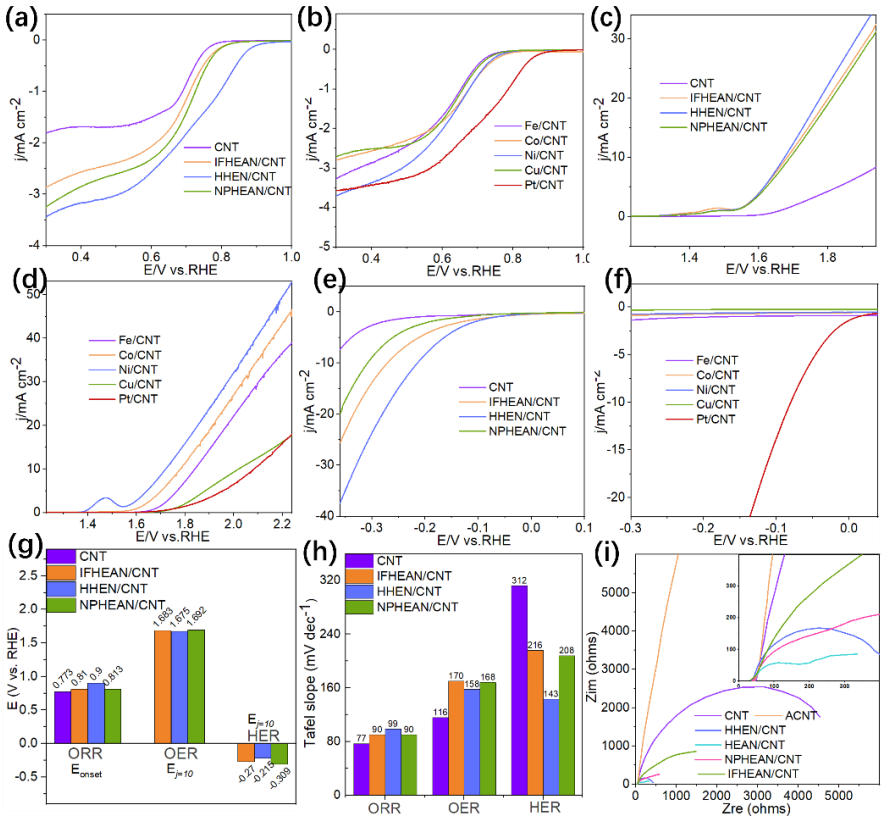

Fig. S11. (a and b)) ORR, (c and d) OER and (e and f) HER polarization LSV curves, (g) overpotential, (h) Tafel plots and (i) EIS for different samples.

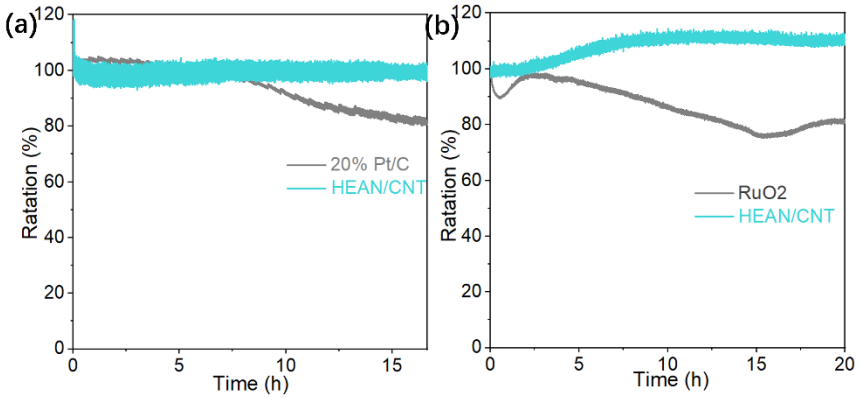

Fig. S12. (a and b) ORR and OER stability test for HEAN/CNT and commercial catalyst.

The long-term stability of the material was also tested by the chronoamperometry method, as shown in **Fig. S12a**, there was no significant attenuation of the HEAN/CNT during the cycle of up to 16 hours, but the 20% Pt/C began to gradually decay after 6h. It can also be seen in **Fig. S12b** that the retention rate of HEAN/CNT has not decayed during the test for up to 20h, but has been more increased and more stable and has been maintained at 110%, but RuO_2 is almost unstable and has been attenuated in the test, demonstrating the excellent stability of the high-entropy material. It also proves the stability brought by the hysteretic diffusion effect.

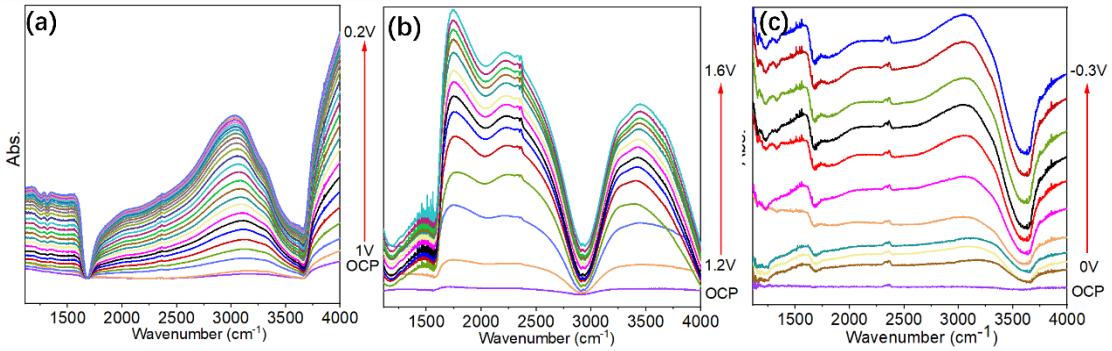

Fig. S13. (a, b and c) in-situ FTIR spectra of HEN for the ORR, OER and HER.

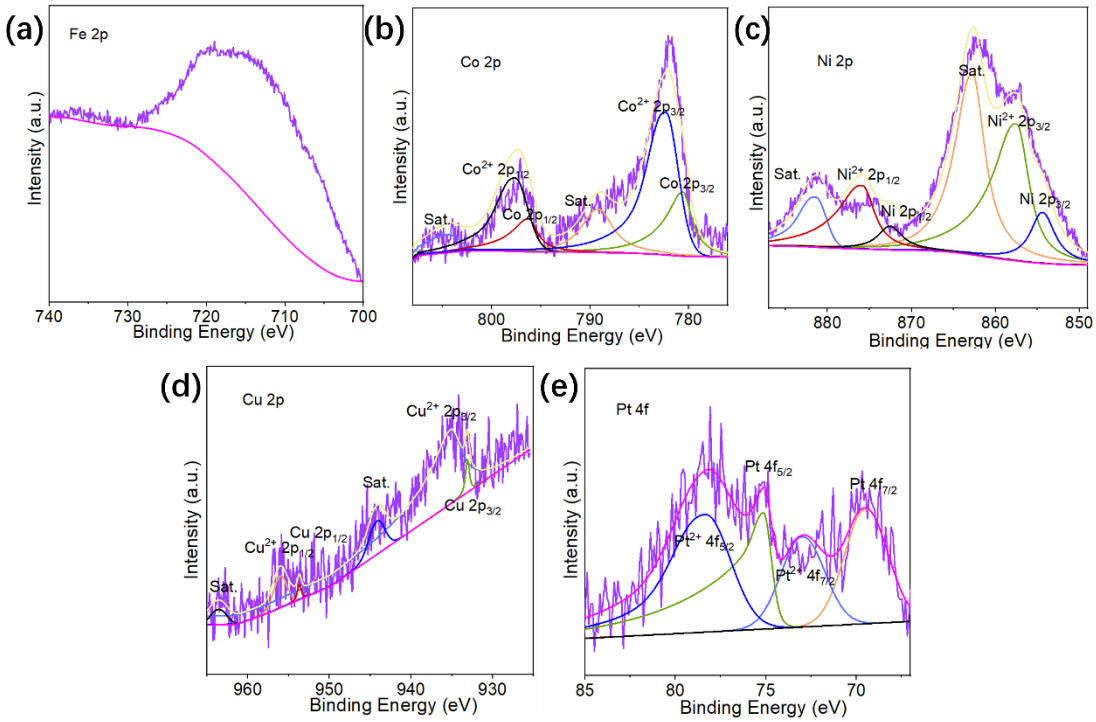

Fig. S14. XPS for OER-catalyzed HEAN/CNT.

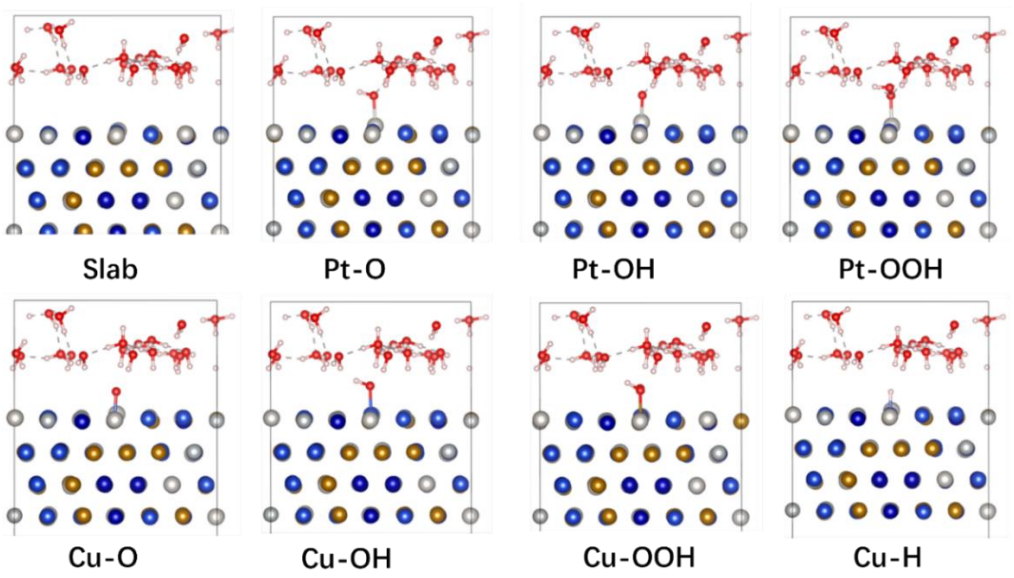

Fig. S15. Various intermediates on active site in explicit solvation.

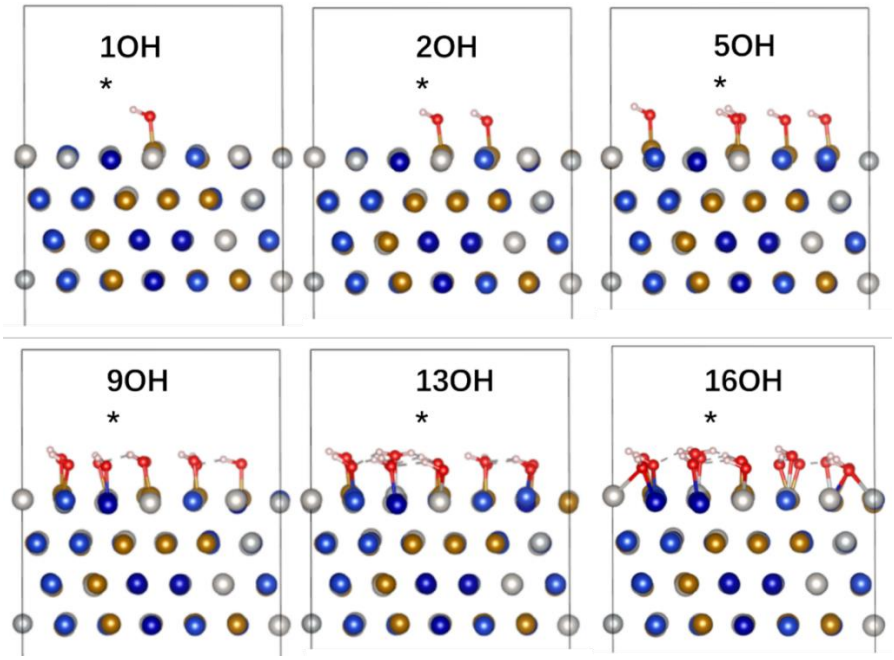

Fig. S16. Optimized OH^- covered surface of HEANs.

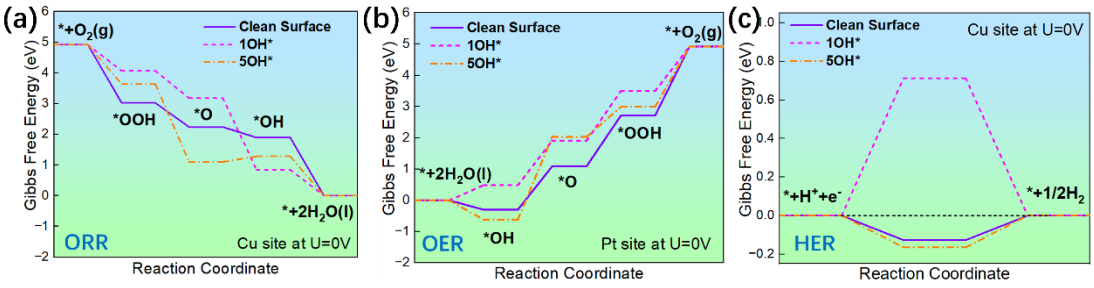

Fig. S17. Gibbs free energy of ORR, OER, and HER on OH^- covered surface.

Supporting Tables.

Table S1. The content of different elements for EDS maps

Z	Element	Family	Atomic Fraction (%)	Atomic Error (%)	Mass Fraction (%)	Mass Error (%)	Fit Error (%)
6	C	K	63.30	1.62	15.88	1.13	1.76
8	O	K	6.24	1.18	2.08	0.43	1.16
26	Fe	K	4.66	0.35	10.11	0.46	0.61
27	Co	K	3.00	0.13	9.22	0.18	1.68
28	Ni	K	8.45	1.16	10.36	1.54	0.34
29	Cu	K	4.70	0.38	11.59	0.56	0.90
78	Pt	L	9.65	1.44	40.76	2.69	0.14

Table S2. DFT energies for different HEANs structures

DFT energy	POSCAR Number	DFT energy	POSCAR Number	DFT energy	POSCAR Number	DFT energy	POSCAR Number
-707.89	179	-705.908	49	-705.128	81	-704.08	173
-707.561	193	-705.856	106	-705.124	67	-704.078	18
-707.346	91	-705.845	160	-705.12	40	-704.017	95
-707.124	105	-705.833	68	-705.119	175	-703.989	96
-707.029	42	-705.832	89	-705.106	151	-703.955	114
-706.947	190	-705.827	180	-705.102	167	-703.834	123
-706.943	127	-705.801	247	-705.089	138	-703.812	154
-706.94	132	-705.799	39	-705.064	189	-703.796	59
-706.875	29	-705.798	94	-705.063	199	-703.695	235
-706.72	163	-705.794	142	-705.058	213	-703.669	87
-706.701	77	-705.789	153	-705.05	136	-703.655	222
-706.643	33	-705.765	75	-704.987	166	-703.543	120
-706.616	30	-705.752	171	-704.98	32	-703.451	5
-706.59	225	-705.748	112	-704.975	66	-703.42	207
-706.583	125	-705.73	22	-704.953	60	-703.379	224
-706.563	28	-705.722	64	-704.908	203	-703.211	218
-706.532	220	-705.721	165	-704.883	41	-703.112	214
-706.502	102	-705.717	168	-704.865	156	-703.057	215
-706.484	135	-705.693	2	-704.845	141	-703.057	249
-706.484	113	-705.692	185	-704.844	181	-702.915	221
-706.468	157	-705.684	80	-704.805	21	-702.717	250

-706.435	46	-705.678	56	-704.805	92	-702.442	223
-706.425	137	-705.668	101	-704.803	186	-702.366	236
-706.396	63	-705.667	129	-704.778	9	-702.09	243
-706.388	16	-705.651	161	-704.778	35	-702.071	237
-706.379	37	-705.645	198	-704.771	26	-702.07	238
-706.376	85	-705.644	58	-704.759	83	-702.046	231
-706.336	131	-705.639	147	-704.739	1	-701.94	242
-706.313	71	-705.633	79	-704.736	194	-701.809	233
-706.298	150	-705.626	107	-704.692	122	-701.807	208
-706.215	14	-705.618	155	-704.691	55	-701.693	204
-706.188	246	-705.599	110	-704.684	162	-701.41	227
-706.152	57	-705.586	27	-704.683	104	-701.092	240
-706.138	90	-705.583	109	-704.674	93	-701.072	239
-706.129	133	-705.576	10	-704.662	73	-700.975	212
-706.127	69	-705.558	191	-704.65	99	-700.862	248
-706.125	44	-705.554	11	-704.637	117	-700.823	202
-706.113	36	-705.552	15	-704.633	228	-700.666	234
-706.098	146	-705.551	84	-704.627	188	-700.594	219
-706.089	124	-705.547	195	-704.625	7	-700.303	216
-706.065	121	-705.543	24	-704.623	174	-700.203	229
-706.055	25	-705.535	177	-704.618	17	-699.799	241
-706.042	43	-705.534	52	-704.603	119	-699.662	226
-706.041	6	-705.532	140	-704.56	53	-698.101	201
-705.998	152	-705.521	158	-704.556	115	-697.479	210
-705.985	82	-705.515	139	-704.545	70	-696.39	232
-705.959	116	-705.498	184	-704.538	196	-694.251	217
-705.955	19	-705.492	103	-704.521	169	-693.354	245
-705.953	86	-705.492	149	-704.495	144	-705.197	206
-705.935	118	-705.48	8	-704.488	192	-705.191	74
-705.923	230	-705.475	3	-704.473	48	-705.178	178
-705.912	76	-705.468	183	-704.466	148	-705.176	13
-705.326	143	-705.467	4	-704.422	130	-705.169	47
-705.29	159	-705.464	100	-704.395	97	-705.161	128
-705.289	51	-705.435	72	-704.393	108	-705.158	0
-705.277	176	-705.429	134	-704.353	65	-705.156	172
-705.256	23	-705.422	145	-704.352	187	-705.151	98
-705.254	78	-705.401	54	-704.303	209	-705.139	62
-705.248	205	-705.381	197	-704.283	170	-705.33	31
-705.241	61	-705.372	45	-704.283	20	-705.329	111
-705.222	34	-705.349	50	-704.218	12	-704.124	211
-705.222	38	-705.349	88	-704.141	182		
-705.207	126	-705.34	164	-704.128	244		

Table S3. DFT energy of various intermediates on active sites

Vacuum					
Active Sites	**Slab (eV)**	***OH (eV)**	***O (eV)**	***OOH (eV)**	***H (eV)**
Co	-867.259	-878.837	-874.447	-883.265	-871.639
Cu	-867.259	-878.046	-872.515	-882.976	-871.026
Fe	-867.259	-879.136	-876.209	-883.679	-872.227
Ni	-867.259	-878.626	-873.499	-882.975	-871.605
Pt	-867.259	-878.380	-873.593	-882.788	-871.960
Implicit Solvation (E_{sol} = 0.1 eV)					
Active Sites	**Slab (eV)**	***OH (eV)**	***O (eV)**	***OOH (eV)**	***H (eV)**
Cu	-867.359	-877.991	-872.561	-883.114	-870.967
Pt	-867.359	-878.419	-873.627	-882.867	--
Explicit Solvation (E_{sol} = 273.86 eV)					
Active Sites	**Slab (eV)**	***OH (eV)**	***O (eV)**	***OOH (eV)**	***H (eV)**
Cu	-1141.116	-1151.764	-1146.413	-1156.488	-1144.832
Pt	-1141.163	-1152.392	-1147.836	-1156.597	--

Table S4. Oxygen adsorption on active sites of HEANs through end-on formats.

Active Sites	**Slab (eV)**	***O_2 (eV)**	**E_{ads} (eV)**	**Magnetization of O_2 (|μ|)**	**d_{o-o}(Å)**
O_2 (g)	**--**	**--**	**--**	1.68	1.233
Co	-867.259	-878.76	-1.581	0.48	1.304
Cu	-867.259	-877.589	-0.410	1.16	1.281
Fe	-867.259	-879.28	-2.101	0.32	1.287
Ni	-867.259	-878.364	-1.185	0.82	1.295
Pt	-867.259	-878.244	-1.065	0.84	1.289

Table S5. The correction of Zero-point vibration and entropy to the Gibbs free energy of intermediates.

Model	**ZPE (eV)**	**T*S (eV)**	**ZPE-T*S (eV)**
*OH	0.34	0	0.34
*O	0.07	0	0.07
*OOH	0.44	0	0.44
H_2(g)	0.27	0.4	-0.13
H_2O(l)	0.57	0.67	-0.1
O_2(g)	-9.92	0	0

Table S6. ICP-MS results of the electrolyte before/after the ORR, OER and HER test with HEAN/CNT loading on 1 cm^2 carbon cloth as the working electrode*.

	Ni ppm	Co ppm	Cu ppm	Pt ppm	Fe ppm
Before test	0.000864	0.000355	0.001050	0.005944	0.052342
After test ORR	0.000895	0.001725	0.013205	0.016833	0.041610
After test OER	0.000932	0.000660	0.014099	0.009875	0.060230
After test HER	0.001184	0.001327	0.004006	0.001616	0.037781

**The lowest concentration of a substance that can be reliably reported by ICP-MS.*

Each electrode was used for the ORR, OER and HER test up to 3000 cycles, thus the post-test electrolyte was obtained.

Table S7.the ECSA, specific and mass activity towards ORR at 0.9V vs. RHE with 1600rpm at a sweep rate of 10 mV s^{-1}.

	ECSA (cm^2)	MA (mA cm^{-2} mg^{-1})	SA (mA cm^{-2})
HEAN/CNT	42.5	2	0.047
20%Pt/C	210	13.4	0.063
HEAN/CNT after 5000CV	42.5	2	0.047
20%Pt/C after 5000CV	210	6.4	0.030

Table S8.the activity normalized by noble metal mass towards OER and HER with 1600rpm at a sweep rate of 10 mV s^{-1}.

	OER of j@1.6V(cm^2)	HER of j@-0.04V
HEAN/CNT	3290(mA cm^{-2} mg_{pt}^{-1})	3733(mA cm^{-2} mg_{pt}^{-1})
20%Pt/C	253(mA cm^{-2} mg_{Ru}^{-1})	1067(mA cm^{-2} mg_{pt}^{-1})

Table S9. Comparison of the trifunctional ORR/OER/HER electrocatalytic performances of the HEAs with previously reported advanced catalysts.

Catalysts	ORR_{Eonset} (V vs. RHE)	$OER_{E=10}$ (V vs. RHE)	$HER_{E=10}$ (V vs. RHE)	Ref.
HEAN	0.913	1.606	-0.035	This work
20%Pt/C	0.997	--	-0.031	This work
RuO_2	--	1.593	--	This work
HEAN after 5000CV	0.908	1.601	-0.034	This work
20%Pt/C after 5000CV	0.944	--	-0.061	This work
RuO_2 after 5000CV	--	1.598	--	This work
HESAC	0.999	--	--	*Nat. Commun.* **2022**, 13, 5071 [10]
Co-N-CTS	0.96	1.51	--	*Nat. Commun.* **2023**, 14, 2294 [11]
FeNiCoCrMn-G	--	1.459	-0.21	*Adv. Sci.* **2021**, 8, 2002446 [12]
Ru1Ni1-NCNFs	--	1.52	-0.035	*Adv. Sci.* **2020**, 7, 1901833 [13]
FeCoNiMnRu/CNFs	--	1.375	-0.005	*Nat. Commun.* **2023**, 14, 2294 [14]
HEA-NPs-(14)	0.92	--	-0.018	*Adv. Mater.* [15],

Appendix

POSCAR179\(1\1\1)

1.00000000000000

15.1250000000000000 0.0000000000000000 0.0000000000000000

-7.5571042706000000 13.1443285683000006 0.0000000000000000

0.0000000000000013 0.0000000000000023 21.3419990539999986

Pt Co Cu Ni Fe

26 26 30 30 32

Selective dynamics

Direct

0.3316000100000025	0.6697800159999971	0.3550899999999970	F	F	F
0.9974696142598509	0.0032738969877585	0.6480948992585941	T	T	T
0.2743024356284560	0.5541232759423088	0.5450500025503628	T	T	T
0.2721901393564199	0.7221676007001649	0.5472089702233960	T	T	T
0.3338699939999970	0.1636999990000021	0.3514899999999983	F	F	F
0.9978178471955046	0.4955426108949886	0.6435593176494544	T	T	T
0.1078306053027787	0.8801150370172451	0.5423470283553126	T	T	T
0.3324899970000033	0.4941099879999982	0.3557699999999997	F	F	F
0.9993349417589792	0.8285380760372300	0.6474785432018952	T	T	T
0.1064880433262544	0.0596005104025181	0.5424370846812926	T	T	T
0.2758684866336824	0.0552013814133086	0.5454817403838738	T	T	T
0.4522704979961007	0.5569410825307883	0.5472259628056994	T	T	T
0.6686499710000007	0.1701499970000029	0.3588099999999983	F	F	F
0.3281511341500304	0.5034854581282232	0.6548120463770910	T	T	T
0.6681500079999978	0.9941599969999970	0.3534099999999967	F	F	F
0.3295826151548015	0.3274685601675354	0.6443059530355011	T	T	T
0.4530211954415915	0.8892984391862018	0.5459666736610584	T	T	T
0.5604299900000029	0.2782199979999973	0.4458599980000031	F	F	F
0.4512225675208906	0.0588245627749456	0.5482648179252761	T	T	T
0.6194794084384783	0.3967327759592523	0.5483420546338663	T	T	T
0.4439891870266924	0.2289746717424890	0.5492222257229111	T	T	T
0.0004700000000000	0.3320699929999975	0.3563199999999966	F	F	F
0.6631353503032275	0.6644623090710369	0.6470876453393635	T	T	T
0.0553699989999998	0.6102799769999976	0.4486500020000008	F	F	F
0.7778017034185304	0.2204599466610107	0.5444736225617024	T	T	T
0.8913199899999995	0.7771499750000004	0.4501899999999992	F	F	F
0.2175700069999991	0.6080800289999999	0.4489500000000035	F	F	F
0.2196400019999984	0.4389899970000002	0.4497300009999989	F	F	F
0.5047500129999989	0.8354700209999990	0.3524999999999991	F	F	F
0.1711340349665348	0.1647827734293418	0.6396085865919531	T	T	T
0.2215400039999977	0.7834500069999990	0.4491000020000016	F	F	F
0.1040440868873021	0.7140373347427426	0.5478963560594767	T	T	T
0.3349199889999994	0.9996200200000018	0.3545900000000017	F	F	F

0.9977194202743768	0.3341254293669413	0.6377987555143128	T	T	T
0.4529313350818412	0.7262887803272018	0.5502274528788937	T	T	T
0.6189815095170978	0.8906452553657971	0.5464264942020871	T	T	T
0.5588300229999987	0.9449300169999972	0.4482000020000001	F	F	F
0.7203099729999991	0.9428399800000022	0.4527499969999980	F	F	F
0.7270200250000016	0.1083799970000001	0.4523700029999986	F	F	F
0.7276499869999995	0.4485200049999989	0.4480200040000000	F	F	F
0.6164548706009512	0.2278000747750478	0.5496739067951424	T	T	T
0.7231900100000033	0.6093299979999998	0.4468500019999979	F	F	F
0.7238799929999971	0.7785900240000032	0.4463000000000008	F	F	F
0.4420631246220231	0.3892591886090953	0.5443532510562326	T	T	T
0.9969099759999978	0.4993599949999989	0.3531100000000009	F	F	F
0.6597165747095004	0.8332126391016391	0.6386813791939956	T	T	T
0.0550299989999985	0.4442299899999966	0.4537699970000020	F	F	F
0.8849700089999999	0.6086099739999966	0.4511699970000009	F	F	F
0.8869699839999967	0.4440500139999983	0.4524599980000019	F	F	F
0.1689999999999969	0.9976999759999998	0.3540100000000024	F	F	F
0.8336101956169237	0.3358100674969903	0.6374937605316390	T	T	T
0.0622700010000017	0.9489399790000022	0.4463300029999999	F	F	F
0.3958899969999976	0.6166499850000022	0.4505899990000017	F	F	F
0.3929100040000009	0.7807899709999973	0.4493900009999976	F	F	F
0.1067097832048230	0.3839731692522347	0.5445472654943492	T	T	T
0.2756292273571632	0.3870755349074088	0.5439773657626839	T	T	T
0.3348299860000026	0.8377599720000006	0.3540300000000016	F	F	F
0.0013079499221310	0.1724046923540260	0.6460821663312192	T	T	T
0.5011900069999982	0.3369199930000022	0.3537400000000019	F	F	F
0.1706243767051447	0.6659027784977696	0.6500154885758235	T	T	T
0.3343400059999979	0.3305799959999973	0.3541700000000034	F	F	F
0.0018828440045268	0.6639943284997711	0.6476864059677906	T	T	T
0.6182409657513332	0.7270873924020548	0.5427663704440483	T	T	T
0.8392000199999998	0.1639100020000015	0.3551300000000026	F	F	F
0.5009746443382320	0.4964902947719556	0.6513246287385426	T	T	T
0.5591199990000035	0.1089800000000025	0.4529799969999999	F	F	F
0.6193692813746398	0.5609785227756485	0.5448354900878369	T	T	T
0.7805291930882619	0.8876361752277439	0.5459211708580717	T	T	T
0.1638099999999980	0.5009199980000005	0.3543999999999983	F	F	F
0.8287860223172913	0.8345221206549869	0.6487921767711067	T	T	T
0.0569799989999993	0.2774499949999978	0.4530299970000016	F	F	F
0.8907899860000015	0.1135599990000031	0.4508400039999998	F	F	F
0.9389792736155914	0.0568086219391212	0.5457157701337237	T	T	T
0.9461087557830349	0.2211690986334627	0.5463334547330080	T	T	T
0.9985200169999970	0.6682900189999970	0.3519300000000030	F	F	F
0.6627556985672906	-0.0000137056905531	0.6472345685431480	T	T	T
0.0008199999999974	0.8335499760000005	0.3528500000000037	F	F	F

0.6631381369064898	0.1652634614004513	0.6487438636439425	T	T	T
0.7821338783767650	0.7226717466184654	0.5492871873678483	T	T	T
0.1682399959999969	0.3275899890000034	0.3531300000000002	F	F	F
0.8335492279010961	0.6608637690402780	0.6456170581030481	T	T	T
0.8926399950000032	0.9482100009999996	0.4502300019999979	F	F	F
0.1133026972918935	0.2263968664423597	0.5485419155185088	T	T	T
0.2781121911478401	0.8874027495369748	0.5450342154366384	T	T	T
0.3889200090000031	0.9448000189999988	0.4480500000000021	F	F	F
0.3889200090000031	0.1075799990000021	0.4471699970000031	F	F	F
0.5102999810000028	0.5042600040000025	0.3545999999999978	F	F	F
0.1760734950477186	0.8362561496757535	0.6426850558076892	T	T	T
0.5072799920000008	0.6711699960000033	0.3567999999999998	F	F	F
0.1736863562316128	0.0036826989971862	0.6490477480966338	T	T	T
0.3861699999999999	0.2790600060000017	0.4504600019999998	F	F	F
0.3901500110000029	0.4410200120000027	0.4505499970000031	F	F	F
0.2215999960000019	0.1112700030000013	0.4464600009999984	F	F	F
0.5611799959999999	0.7827799920000018	0.4504999959999978	F	F	F
0.8379799719999994	0.5012099739999982	0.3562999999999974	F	F	F
0.5000236842564888	0.8350750319234547	0.6453993733246797	T	T	T
0.6173634649342022	0.0543946160027109	0.5482507158093756	T	T	T
0.5630599859999990	0.6144999859999984	0.4475900010000018	F	F	F
0.5588399769999981	0.4488700030000032	0.4489800030000026	F	F	F
0.8405600190000015	0.0014200000000031	0.3575999999999979	F	F	F
0.5068053963430380	0.3363795279011839	0.6476820717890047	T	T	T
0.1645199949999991	0.6702100039999976	0.3514199999999974	F	F	F
0.8250192661220676	-0.0014705088650812	0.6401286275327662	T	T	T
0.0586199979999975	0.7782099840000001	0.4467500000000015	F	F	F
0.1696799990000031	0.8337000009999969	0.3537200000000027	F	F	F
0.8329163841085282	0.1653852128994819	0.6411851216276453	T	T	T
0.9423921237554268	0.8866448205841344	0.5477568335625635	T	T	T
0.7852012700102498	0.5588806558143298	0.5452992535155238	T	T	T
0.1666299999999978	0.1642699989999983	0.3517000000000010	F	F	F
0.8282910470880458	0.4950072095011696	0.6398198683276106	T	T	T
0.0060799999999972	0.9999399780000005	0.3549500000000023	F	F	F
0.6692263322495772	0.3324896579061563	0.6437997487322447	T	T	T
0.4986000059999967	0.0003799999999998	0.3572100000000020	F	F	F
0.1650312122548274	0.3376998751609370	0.6409582434081549	T	T	T
0.1037483394936662	0.5499072588789942	0.5459353940868286	T	T	T
0.4968200030000034	0.1589699980000034	0.3521900000000002	F	F	F
0.1579234594856038	0.4884847357282595	0.6381710067101539	T	T	T
0.2234500049999966	0.9431999919999967	0.4444300010000006	F	F	F
0.2199900000000028	0.2723099890000000	0.4533099980000017	F	F	F
0.2758110399973612	0.2268205414191925	0.5422973908203896	T	T	T
0.8352500199999966	0.3419899940000022	0.3581100000000035	F	F	F

0.5011995765427959	0.6800304791003479	0.6396231538996976	T	T	T
0.6751400229999973	0.5051100250000005	0.3572699999999998	F	F	F
0.3406347302526551	0.8423549732851484	0.6414234041405263	T	T	T
0.8266800050000001	0.6627200249999987	0.3575599999999994	F	F	F
0.4891395700769358	0.9982187969440887	0.6440395371125874	T	T	T
0.6807900069999988	0.3432399929999974	0.3552800000000005	F	F	F
0.3461879184103683	0.6756688732747290	0.6405358867252983	T	T	T
0.7350400090000022	0.2913100119999967	0.4497399999999985	F	F	F
0.6736000180000019	0.6697400210000026	0.3585100000000025	F	F	F
0.3364027337269572	-0.0014994257630148	0.6419686155030475	T	T	T
0.6718999739999987	0.8302800060000024	0.3593699999999984	F	F	F
0.3327918413020804	0.1616587987825028	0.6442932158017260	T	T	T
0.8296599979999968	0.8305000069999977	0.3552099999999996	F	F	F
0.4947342340963994	0.1627764080001075	0.6425105670484738	T	T	T
0.8871499899999975	0.2872700100000003	0.4504799990000024	F	F	F
0.7713185082808274	0.0492534245554822	0.5469611706445343	T	T	T
0.7863593407936236	0.3923635568492818	0.5437910186748114	T	T	T
0.9436677020097785	0.3922240136663086	0.5426625345190975	T	T	T
0.9419481585628224	0.5547145410328402	0.5438168561207971	T	T	T
0.9478899132669776	0.7126345554844623	0.5458100958188259	T	T	T
0.0081699999999998	0.1646000000000001	0.3576300000000003	F	F	F
0.6700153615289407	0.4991086337754980	0.6425228195242664	T	T	T
0.0636899989999975	0.1185199990000001	0.4431599970000022	F	F	F

SI References

[1] G. Kresse, J. Furthmüller, Efficiency of ab-initio total energy calculations for metals and semiconductors using a plane-wave basis set. *Computational Materials Science* **1996**, 6, 15.

[2] G.Kresse, J. Furthmüller, Efficient iterative schemes for ab initio total-energy calculations using a plane- wave basis set. *Phys. Rev. B* **1996**, 54, 11169.

[3] John P. Perdew, Kieron Burke, and Matthias Ernzerhof, Generalized Gradient Approximation Made Simple. *Phys. Rev. Lett.* **1996**, 77, 3865.

[4] Egill Skulason, Vladimir Tripkovic, Mårten Björketun, Sigridur Gudmundsdottir, Gustav Karlberg, Jan Rossmeisl, Thomas Bligaard, Hannes Jonsson, Jens Kehlet Nørskov, Modeling the Electrochemical Hydrogen Oxidation and Evolution Reactions on the Basis of Density Functional Theory Calculations. *The Journal of Physical Chemistry C* **2010**, 114, 18182.

[5] Kiran Mathew; Ravishankar Sundararaman; Kendra Letchworth-Weaver; T. A. Arias; Richard G. Hennig, Implicit solvation model for density-functional study of nanocrystal surfaces and reaction Pathways. *J. Chem. Phys*. **2014**,140, 084106.

[6] Youchao Kong, Shanshan Yan, Jinxian Feng, Shuangpeng Wang, Hui Pan, Design of phosphorus-functionalized MXenes for highly efficient hydrogen evolution reaction. *J. Mater. Chem. A*, **2021**, 9, 597-606

[7] Yinghe Zhao, Haobo Li, Ruoou Yang, Shuxian Xie, Teng Liu, Pengyu Li, Youwen Liu, Huiqiao Li, Fa Yang, Tianyou Zhai, Transient phase transition during the hydrogen evolution reaction. *Energy Environ. Sci.* **2023**,16, 3951-3959.

[8] Shah, A.H., Zhang, Z., Huang, Z. *et al.* The role of alkali metal cations and platinum-surface hydroxyl in the alkaline hydrogen evolution reaction. *Nature Catalysis* **2022**, 5, 923-933.

[9] Liu, K., Fu, J., Lin, Y. *et al.* Insights into the activity of single-atom Fe-N-C catalysts for oxygen reduction reaction. *Nature Communications* **2022**, 13, 2075.

[10] Rao, P., Deng, Y., Fan, W. *et al.* Movable type printing method to synthesize high-entropy single-atom catalysts. *Nat. Commun.* **2022**, 13, 5071.

[11] Shi, W., Li, Z., Gong, Z. *et al.* Transient and general synthesis of high-density and ultrasmall nanoparticles on two-dimensional porous carbon via coordinated carbothermal shock. *Nat. Commun.* **2023**, 14, 2294.

[12] T. X. Nguyen, Y.-H. Su, C.-C. Lin, J. Ruan, J.-M. Ting, A New High Entropy Glycerate for High Performance Oxygen Evolution Reaction. *Adv. Sci.* **2021**, 8, 2002446.

[13] M. Li, H. Wang, W. Zhu, W. Li, C. Wang, X. Lu, RuNi Nanoparticles Embedded in N-Doped Carbon Nanofibers as a Robust Bifunctional Catalyst for Efficient Overall Water Splitting. *Adv. Sci.* **2020**, 7, 1901833.

[14] Hao, J., Zhuang, Z., Cao, K. *et al.* Unraveling the electronegativity-dominated intermediate adsorption on high-entropy alloy electrocatalysts. *Nat. Commun.* **2022**, 13, 2662.

[15] Wang Y, Luo W, Gong S, Luo L, Li Y, Zhao Y, Li Z. Synthesis of High-Entropy-Alloy Nanoparticles by a Step-Alloying Strategy as a Superior Multifunctional Electrocatalyst. *Adv. Mater.*, **2023**, e2302499.